

Extended Czjzek model applied to NMR parameter distributions in sodium metaphosphate glass

Filipe Vasconcelos* and Sylvain Cristol, Jean-François Paul, Laurent Delevoye
Unité de Catalyse et Chimie du Solide, UMR CNRS 8181, École Nationale Supérieure de Chimie de Lille,
Université de Lille, BP 108, 59652 Villeneuve d'Ascq Cedex, France

Francesco Mauri
Institut de Minéralogie et Physique des Milieux Condensés,
Université Pierre et Marie Curie, Campus Boucicaut, 140 rue de Lourmel, 75015 Paris

Thibault Charpentier
CEA, IRAMIS, SIS2M, CEA/CNRS UMR 3299 - Laboratoire de Structure et
Dynamique par Résonance Magnétique F-91191 Gif-sur-Yvette cedex, France

Gérard Le Caër
Institut de Physique de Rennes, UMR URI-CNRS 6251,
Université de Rennes 1, Campus de Beaulieu, Bât 11A,
Avenue du Général Leclerc, F-35042 Rennes Cedex, France
(Dated: March 16, 2018)

The Extended Czjzek Model (ECM) is applied to the distribution of NMR parameters of a simple glass model (sodium metaphosphate, NaPO_3) obtained by Molecular Dynamics (MD) simulations. Accurate NMR tensors, Electric Field Gradient (EFG) and Chemical Shift Anisotropy (CSA), are calculated from Density Functional Theory (DFT) within the well-established PAW/GIPAW framework. Theoretical results are compared to experimental high-resolution solid-state NMR data and are used to validate the considered structural model. The distributions of the calculated coupling constant $C_Q \propto |V_{zz}|$ and of the asymmetry parameter η_Q that characterize the quadrupolar interaction are discussed in terms of structural considerations with the help of a simple point charge model. Finally, the ECM analysis is shown to be relevant for studying the distribution of CSA tensor parameters and gives new insight into the structural characterization of disordered systems by solid-state NMR.

Keywords:

I. INTRODUCTION

It is generally accepted, since the early work of Zachariassen,¹ that oxide glasses are built up from polyhedra randomly organised in such a way however that the local short-range order that prevails in the corresponding crystalline compounds is preserved. This seminal model, named the Continuous Random Network (CRN), evolved slightly with time and was extended to covalent glasses such as amorphous silicon (Refs. 2,3 and references therein). Its validity appears to be reinforced by diffraction techniques from which radial distribution function (RDF) can be determined and compared to the radial distribution associated with the local arrangements of polyhedra in a CRN model. However, conclusions about the structures of amorphous materials are questionable when they are obtained solely from pair correlations as they suffer from a lack of uniqueness beyond very short range structure². Other techniques that are more sensitive to topological or medium-range order are needed to constrain structural models as advocated very recently for amorphous silicon^{2,3}. Complementary techniques are then needed to provide additional input data which constrain models determined for instance by Reverse Monte Carlo methods. Among the various spectroscopic techniques that can be used (Raman, Infrared, EXAFS for instance), Solid State Nuclear Magnetic Resonance (NMR) spectroscopy can be seen as one of the most promising tools to characterise oxide glass structure.

In solid-state NMR, the structural information is carried

by the different interactions, i.e. chemical shift, quadrupolar, dipolar coupling, indirect spin-spin coupling, which are deduced either directly by a one-dimensional experiment or indirectly through the use of multiple-dimensional experiments (homo and hetero-nuclear correlations). These interactions being orientationally dependent, they often contribute to a line-broadening of NMR spectra. All these interactions can be described by tensors, i.e., chemical shift anisotropy tensor (CSA), Electric Field Gradient tensor (EFG). If the anisotropic parts of NMR interactions have been for a long time considered as a major drawback for the NMR investigation of solids, the development of Magic Angle Spinning (MAS) technique has open new perspectives by significantly improving the spectral resolution, especially for those nuclei with a spin half value ($I = 1/2$). For nuclei with higher spin values ($I > 1/2$), which are subjected to the quadrupole interaction, MAS technique alone is unable to average out completely the quadrupolar interaction. Over the last twenty years, several methods were proposed to get rid of the second-order anisotropic quadrupolar interactions: Double Orientation Rotation (DOR),⁴ Dynamic-Angle Spinning (DAS),⁵ Multiple-Quantum-MAS (MQMAS),^{6,7} or satellite-transition MAS (STMAS).⁸ The most versatile and most widely used MQMAS method is a high-resolution experiment designed for half-integer quadrupolar nuclei and routinely used to average out the anisotropic second-order quadrupolar interactions by correlating the multiple-quantum transitions with the single quantum transitions. These methods, among others, allow

nowadays the observation of many nuclei from the periodic table and the characterisation of their anisotropic interaction tensors.

In crystalline solids, the broadening of NMR spectra of powdered samples is the result of different orientations of the crystallites relative to the external field. In such a case, the structural characterisation can be done without ambiguity from the principal components of the tensors alone. In the case of an amorphous system, the distribution of chemical environments results in an intrinsic distribution of all the components of the interaction tensor. This additional distribution is then responsible for the broadening of the spectra observed experimentally in glasses. The challenging problem in solid-state NMR analysis of disordered materials is to interpret this spectral broadening in structural terms. First, the extraction of NMR parameter distributions from NMR data can be rather difficult. It is clear that the availability of analytical models can facilitate this task. Second, the relationships between NMR parameter distributions and the structural and chemical disorder has to be established.

Structure elucidation by solid-state NMR suffers from a fundamental drawback: *the assignment of NMR spectra to chemical environments is an indirect process*. Thereby, except for some cases where the chemical environments belong clearly to very different families, the assignment needs a structural model to remove possible ambiguities. The development of methods to calculate NMR parameters from the atomic-scale during the last decade is this view as they allow the assignment of similar chemical environments and confirm the sensibility of NMR parameters to structure. In particular, the now routinely used DFT-PAW/GIPAW (Projector Augmented Wave and Gauge Including Projector Augmented Wave respectively)^{9,10} combined approach accounts very accurately for the CSA and EFG tensors of a large amount of crystalline organic^{11,12} or inorganic^{10,13–16} compounds. However, this theoretical approach to assign resonances is still an indirect process. Indeed, for crystalline compounds, a known structure, deduced from diffraction techniques, is mandatory to be used as an input in *ab initio* and DFT codes and to further be compared to experimental NMR results. Similarly, for amorphous or disordered compounds, structural model must be built to confirm the interpretation of NMR spectra. Recently, the combination of molecular dynamics (MD) and solid-state NMR has shown a great ability to interpret experimental spectra and to propose structural glass models for different oxide glasses^{17–23}. This approach has the advantage to give access to the distributions of all the NMR interaction tensors (CSA, EFG).

The case of EFG tensor distribution has been recently subject to some new considerations in the context of solid-state NMR. Indeed, D’Espinose de Lacaillerie *et al.*²⁴ examined the fields of applications of the Czjzek model^{25,26}, also called Gaussian Isotropic Model (GIM) that is summarized in the background section (Section II). The GIM is the first analytical model for the analysis of NMR lineshapes observed in the MAS NMR spectra of quadrupolar nuclei in disordered solids. Apart from its application in other spectroscopies (ex. in Mössbauer spectroscopy Ref. 26,27 and references therein),

this model was successfully applied to the NMR study of amorphous systems, to different nuclei such as aluminium-27^{24,28,29}, gallium-71^{30–33}, arsenic-75³² and should be applicable to other nuclei (sodium shows characteristic isotropic distributions see ex. Fig. 2 of Ref. 34). In particular, this model is able to describe the asymmetric broadening observed at low chemical shift^{24,33}. Since a quadrupolar nucleus in an amorphous system presents also a distribution of the isotropic chemical shift, the GIM gives the means to better separate and quantify these two contributions within the resonance broadening. However, the specific two hypotheses defining the GIM (i.e., rotational invariance and central limit theorem)^{26,35} are unable to provide structural considerations from the analysis of the NMR lineshape distribution. As discussed by Le Caër *et al.*,³⁵ the GIM, which results *in fine* from the application of a central limit theorem to the EFG tensor (section II B), can thus be seen as a kind of “black hole” from *which no information about the specific structural features of the investigated solid and about the physical origins of the EFG can come*.

The introduction of the Extended Czjzek Model (ECM),^{26,35,36} also summarized in Section II, is currently the simplest but useful way to generalise the GIM. In a recent contribution, one of us showed that this ECM could be seen as the introduction of physical (i.e., structural) contribution to the GIM. Indeed, the ECM *is intended to mimic the EFG contribution of a well-defined neighbourhood of a given atomic species modified by the effect of more remote atomic shells*. In practice, this well-defined first atomic shell and the remote atomic shells are modelled by a fixed “local” contribution and a distributed Czjzek contribution, respectively. Therefore, depending on the relative weight of the local contribution, the ECM is able to include some direct structural effects in the Czjzek model. Indeed, for a given EFG tensor, the relation between structural data and the quadrupolar interaction can be easily determined from *ab initio* calculations of the EFG²⁴. Then, the observation of an ECM distribution with a predominant local contribution can be interpreted through structural considerations.

In this paper, we present a general approach to study the EFG distribution of a simple glass model, namely the sodium metaphosphate glass (NaPO_3), generated by molecular dynamics (MD). In a previous work, the NMR signature of the non-bridging oxygen (NBO) of this compound was interpreted, to some extent, with a continuous random network model³⁷. Indeed, the observed small distribution of the quadrupolar parameters, the mean value of which is comparable to those observed in related crystalline compounds, was interpreted as the conservation of the local structure. In addition, the large distribution of the isotropic chemical shift was interpreted as the signature of long-range disorder. For bridging oxygens (BO), some correlation between the quadrupolar parameters and simple structural properties appeared to be close to those observed in silicates.³⁸ This glass system can thus be seen as a good candidate for the application of the ECM to ^{17}O environments. In a second step, the use of the ECM to describe sodium NMR lineshapes will show the ability of such model to reveal a pure isotropic tensor distribution as defined in the GIM.

This paper is organised as follows. In section II, we recall the basic characteristics of the distributions of the main EFG parameters in the frame of the GIM and ECM. In Section III, we present the methodology used to generate different configurations of the sodium metaphosphate glass and to calculate the NMR parameters for all nuclei in the corresponding glass structure. In section IV, the results are compared to experimental ^{17}O and ^{31}P high-resolved NMR spectra to validate the structural model. In the same section, we present a detailed analysis of the calculated EFG distribution within the ECM. In Section V, we analyse the distributions of the EFG tensor parameters and their link with the structure of the glass. In particular, we show that a simple point charge model analysis is able to explain the distributions related to the EFG tensor for the different sites. In Section VI, we introduce a preliminary application of the ECM to the distribution of the Chemical Shielding Anisotropy tensor.

II. DISTRIBUTION OF THE EFG TENSOR: BACKGROUND

A. EFG related definitions

In solid-state NMR, the quadrupolar interaction is characterised by two parameters: C_Q and η_Q (respectively the quadrupolar coupling constant, and the quadrupolar asymmetry), which are both defined from the three principal components of the diagonal EFG tensor (\mathbf{V}), by the following relations:

$$C_Q = \frac{e|Q|}{h}|V_{zz}|, \quad \eta_Q = \frac{V_{yy} - V_{xx}}{V_{zz}} \quad (1)$$

where e is the elementary charge, h is the Planck's constant, Q is the quadrupolar moment and the principal components V_{ii} , ($i = x, y, z$) are sorted such that $|V_{zz}| \geq |V_{xx}| \geq |V_{yy}|$. In the present work, we used $Q = -25.58 \times 10^{-31} \text{m}^2$ and $Q = 100.54 \times 10^{-31} \text{m}^2$, for respectively the oxygen and the sodium quadrupolar moment as tabulated by Pyykkö³⁹.

Thereafter, we only consider the parameters V_{zz} and η_Q to represent the principal components of the diagonal EFG tensor. Even if NMR experiments at room temperature are unable to provide the sign of the largest principal component⁴⁰, it is explicitly available by DFT calculations and is important to characterize the distribution as demonstrated below.

The EFG tensor, whose components are $v_{i,j}$ with ($i, j = x, y, z$), is usually not diagonal, and three others parameters defining the orientation of the tensor in a fixed reference frame are required. Consequently, the EFG tensor is completely defined by five independent quantities as expected for a traceless symmetric second-rank tensor. Following Czjzek *et al.*²⁵, we define five real parameters U_i from the Cartesian components of the EFG tensor.

$$U_1 = v_{zz}/2, U_2 = \frac{v_{xz}}{\sqrt{3}}, U_3 = \frac{v_{yz}}{\sqrt{3}}, U_4 = \frac{v_{xy}}{\sqrt{3}}, U_5 = \frac{(v_{xx} - v_{yy})}{2\sqrt{3}} \quad (2)$$

The five-dimensional vector $\mathbf{U} = (U_1, \dots, U_5)$ constitutes a

random vector representative of the EFG tensor of an amorphous solid in the same fixed reference frame for all the sites. The distribution of \mathbf{U} fulfils a number of conditions for disordered solids which are statistically invariant by any rotation. This invariance does not imply any kind of local geometrical symmetry. In other words, “statistical isotropy”, which is a global property, and “geometrical anisotropy”, which is a local property, are not contradictory characteristics and are most often the rules for amorphous solids. Statistical isotropy simply means that the distribution of \mathbf{U} remains unchanged when any fixed, but arbitrary, frame of reference is chosen to calculate the EFG's of all atoms of the selected isotope. It implies nothing about possible symmetries of local clusters centered on these atoms. The essential conditions, which are needed in the discussion of the results of the present article, are derived by a simple method in Ref. 26. They are:

- The distribution of \mathbf{U} is such that $\langle U_i \rangle = 0$ and $\langle U_i U_j \rangle = \sigma^2 \delta_{ij}$ with ($i, j = 1, \dots, 5$) where σ^2 is the common variance of the five components of \mathbf{U} . The latter conditions are true for any distribution of \mathbf{U} as soon as means and variances do exist.
- The marginal distribution $P(U_1)$ is a priori asymmetric and different from the marginal distributions $P(U_{k,k>1})$ which are all identical and symmetric.

When structural models are available, theoretical distributions $P(U_i)$ can be used to check if the previous conditions of statistical isotropy hold or not. In addition, when the distribution of \mathbf{U} is multivariate Gaussian, as in the Czjzek model, then the U_i are independent random variables and the five distributions $P(U_i)$ are identical Gaussians.

B. Gaussian Isotropic Model (Czjzek model)

The Czjzek model²⁵ is used for the analysis of the joint distribution of the components of the previous vector $P(U_1, \dots, U_5)$ in the context of an isotropic distribution of the EFG tensor. At the thermodynamic limit (i.e. an infinite number of sites), or at least when the physics that determine the distribution of the EFG tensor meets the quite general requirements of the multidimensional central limit theorem, the random variables U_i become independent and identically distributed according to a Gauss distribution with a zero mean. With these two assumptions, the Czjzek model is summarised by the following analytical expression for the bivariate distribution $P(V_{zz}, \eta_Q)$:

$$P(V_{zz}, \eta_Q) = \frac{1}{(2\pi)^{1/2} \sigma^5} V_{zz}^4 \eta_Q (1 - \eta_Q^2/9) \exp\left(-\frac{S^2}{2\sigma^2}\right) \quad (3)$$

where S is the norm of the tensor ($S^2 = V_{zz}^2(1 + \frac{\eta_Q^2}{3})$). This model is fully defined by a single parameter, namely the standard deviation σ of the Gaussian distribution of every component U_i . In this paper, we only consider some properties of the marginal distributions $f(\eta_Q)$ and $f(V_{zz})$. For further de-

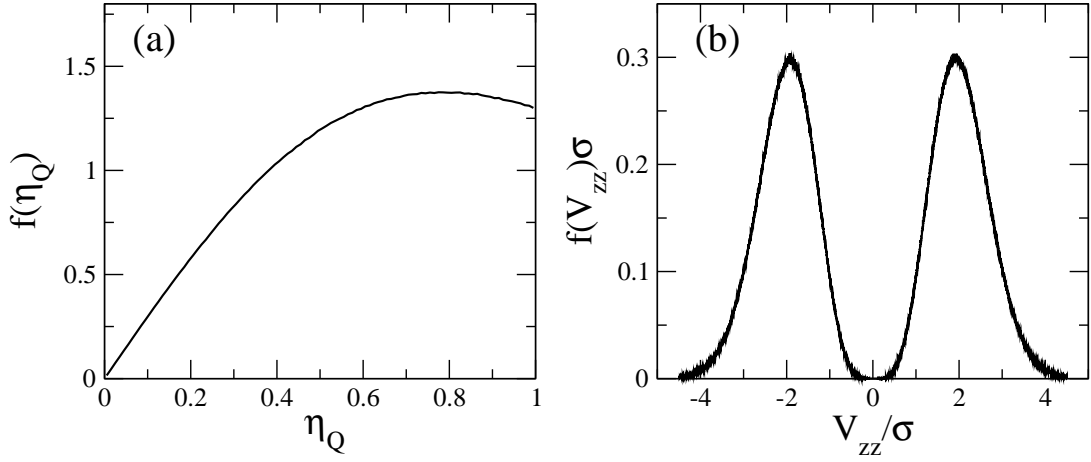


FIG. 1: Characteristic shapes of the marginal distributions of (a) η_Q and (b) V_{zz}/σ in case of a Czjzek distribution of the EFG tensor (GIM). (a) The distribution $f(\eta_Q)$ is independent of σ , the single free parameter of the bivariate distribution of V_{zz} and η_Q ; the mean asymmetry parameter is 0.6098 (b) The V_{zz} distribution is symmetric about zero. The ratio ρ_Z (see Eq. 7) is independent of sigma, being ~ 0.32607 .

scription of the GIM properties, the reader is referred to the following articles (Refs. 24–26 and 35).

Figure 1 presents the characteristic shapes of the marginal distributions $f(\eta_Q)$ and $f(V_{zz})$ obtained from the distribution (3). These distributions have the following properties:

- (A) the shape and the mean value of the $f(\eta_Q)$ distribution are independent of σ (Figure 1 (a)). The latter distribution is given by

$$f(\eta_Q) = 3\eta_Q \frac{1 - \frac{\eta_Q^2}{9}}{\left(1 + \frac{\eta_Q^2}{3}\right)^{5/2}} \quad (4)$$

- (B) The marginal distribution $f(V_{zz})$ is symmetric about zero (Figure 1 (b)) and $f(V_{zz}) \propto V_{zz}^4$ for small values of V_{zz} .

C. Extended Czjzek model

1. Model presentation

The Extended Czjzek Model (ECM) allows the introduction of an anisotropic part in the total EFG tensor. In this model, the total observed EFG tensor $\mathbf{V}(\epsilon)$ is defined as the sum of two distinct contributions as follows:

$$\mathbf{V}(\epsilon) = \mathbf{V}_0 + \rho \mathbf{V}_{\text{GIM}} \quad (5)$$

where \mathbf{V}_0 represents the local anisotropic tensor due to a close neighbourhood of the considered atom and \mathbf{V}_{GIM} is the global isotropic distribution modelled by a GIM tensor weighted by a parameter ρ due to more remote atomic shells. The choice of a Czjzek contribution to express the effect of noise is justified by the two very general assumptions, statistical isotropy and gaussianity, which unavoidably lead to the Czjzek model.

In Eq. 5 the tensor \mathbf{V}_{GIM} is obtained from a vector \mathbf{U} (Eq. 2) whose components are standard Gaussians with means equal to zero and variances equal to 1. All tensors in Eq. 5 are expressed without loss of generality in the local frame of reference in which \mathbf{V}_0 is diagonal (see A and B). Thus, the distribution of $\mathbf{V}(\epsilon)$ is not statistically isotropic. If needed, $\mathbf{V}(\epsilon)$ can be transformed into a tensor $\mathbf{V}'(\epsilon)$ which is statistically isotropic (A). The tensors $\mathbf{V}(\epsilon)$ and $\mathbf{V}'(\epsilon)$ have identical distributions of principal values (B). The distributions of the components of \mathbf{V}'_0 are further discussed in B.

The total EFG tensor is now a function of ϵ , with ρ defined by:

$$\rho = \frac{\epsilon \|\mathbf{V}_0\|}{\|\mathbf{V}_{\text{GIM}}\|} \quad (6)$$

which corresponds to the ratio of the norm of the different contributions. This ϵ parameter permits to study the influence of each contribution independently of the value of the fixed tensor. The principal values of the fixed diagonal tensor \mathbf{V}_0 are fully characterized by $V_{zz}(0)$ and $\eta_Q(0)$. In summary, the ECM is defined by three parameters: $V_{zz}(0)$ and $\eta_Q(0)$ for the local contribution and ϵ for the weight of the noise in the total EFG tensor. Hereafter, \mathbf{V}_0 will be consistently named the “local” contribution to the EFG tensor $\mathbf{V}(\epsilon)$ while the name “noise” (or Czjzek or background) will be used to designate the second contribution.

The main simplification of the ECM is to consider that $\eta_Q(0)$ and $V_{zz}(0)$ are not distributed, being the same for all atoms of a given family. By family, we mean the set of all local clusters, centered on atoms of a given species, which can be put in coincidence by some rotation, within very small atomic displacements (see sections 3 of Ref. 26 and 3.1 of Ref. 35). This simplification aims at restricting the number of free parameters to a minimum value while mimicking the essential structural effects of the local atomic configurations. A disordered solid, for which the ECM is relevant, does not necessarily include a single family of sites. Many families may

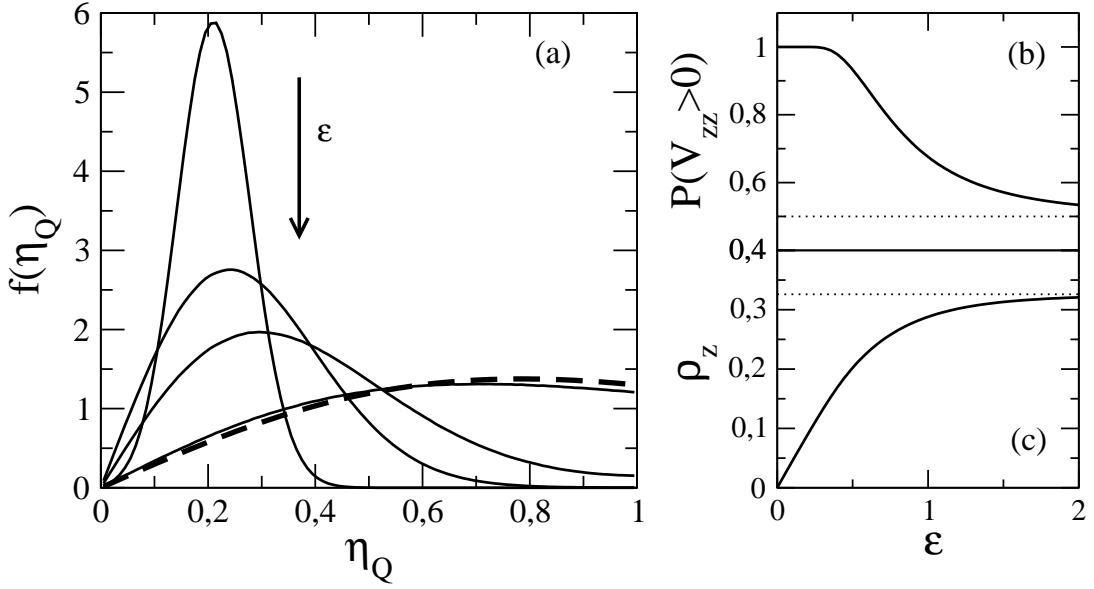


FIG. 2: Evolution of (a) the shape of the η_Q distribution, (b) the probability of occurrence of $V_{zz} > 0$ and (c) the parameter ρ_Z (relation 7) as a function of the parameter ϵ of the ECM. The other ECM parameters are: $\eta_Q(0)=0.2$, $V_{zz}(0)=1$. The dashed lines represents (a) the η_Q distribution and (b) the asymptotical values of $P(V_{zz} > 0)$ and (c) ρ_Z for a Czjzek model.

be necessary to describe the whole set of sites occupied by a given atomic species. A finite collection of extended Czjzek families may be sufficient to describe the EFG properties of some solids while others need to be described by a continuous distribution of families (Appendix B 3).

2. η_Q and V_{zz} distributions within the ECM

We restrict the following discussion to the characteristics of the distributions of η_Q and V_{zz} in the ECM model and we compare them to the related distributions in the Czjzek model as summarized by the previous points (A) and (B). For a detailed description of all the ECM properties, the reader is referred to Ref. 35.

Figure 2 (a) presents the evolution of the distribution $f(\eta_Q)$ of η_Q with ϵ for $\eta_Q(0) = 0.2$. For small values of ϵ (i.e. large local contribution), the distribution of η_Q is narrow and concentrated around $\eta_Q(0)$. For increasing ϵ (i.e. increase of the global isotropic contribution) the distribution $f(\eta_Q)$ converges to the η_Q distribution of the Czjzek model (Eq. 4). For all pairs $(\eta_Q(0), \epsilon)$, the $f(\eta_Q)$ distribution is accurately approximated by a closed-form expression (Eq. 22 of Ref. 35). For a given value of ϵ , the η_Q distributions allow a determination of the parameter $\eta_Q(0)$ of the ECM.

Figure 2 (b,c) presents the evolution with ϵ of two characteristics of the V_{zz} distributions. Figure 2 (b) presents the variation with ϵ of the probability of occurrence of positive values of V_{zz} (i.e $P(V_{zz} > 0)$). A given probability $p = \max(P(V_{zz} > 0), P(V_{zz} < 0))$, with $0.5 \leq p \leq 1$ is not in a one-to-one correspondence with ϵ (see for instance Fig. 6 of Ref. 35). It is thus necessary to select another parameter for an unambiguous determination of ϵ . A convenient parameter, which characterizes

the V_{zz} distribution while being scale independent, denoted ρ_Z , is defined as follows:

$$\rho_Z = \frac{\sigma(|V_{zz}|)}{\langle |V_{zz}| \rangle} \quad (7)$$

where $\sigma(|V_{zz}|)$ and $\langle |V_{zz}| \rangle$ are respectively the standard deviation and the average value of $|V_{zz}|$ distribution. Figure 2 (c) presents the evolution of ρ_Z with ϵ . The ratio ρ_Z is accurately approximated the relation given in (i) below. The previous ratio allows an unequivocal determination of ϵ .

We propose now a simple procedure to analyse, within the ECM, a given distribution of V_{zz} and η_Q . Indeed, as on the one hand the distribution of V_{zz} is practically independent of $\eta_Q(0)$ and depends largely on the $V_{zz}(0)$ value and on the other hand ϵ is completely defined from the V_{zz} distribution, only three steps are needed to determine all the ECM parameters:

- (i) ϵ is determined from ρ_Z using the expression (Eq. 20 of Ref. 35)

$$\rho_Z = 0.32607(1 - \exp(-2.097\epsilon^{1.151}))$$

valid for any $\eta_Q(0)$, where 0.32607 is the value for the Czjzek model.

- (ii) $\eta_Q(0)$ is first determined from the η_Q distribution using the approximation (Eq. 22 of Ref. 35)

$$f(\eta_Q) \propto \eta_Q^\alpha \exp(-k\eta_Q^\beta) + (2 - \eta_Q)^\alpha \exp(-k(2 - \eta_Q)^\beta)$$

with $0 \leq \eta_Q \leq 1$ and where k , α , β are tabulated in Ref. 35 as a function of ϵ .

- (iii) Using the previous parameters, $|V_{zz}(0)|$ is finally well

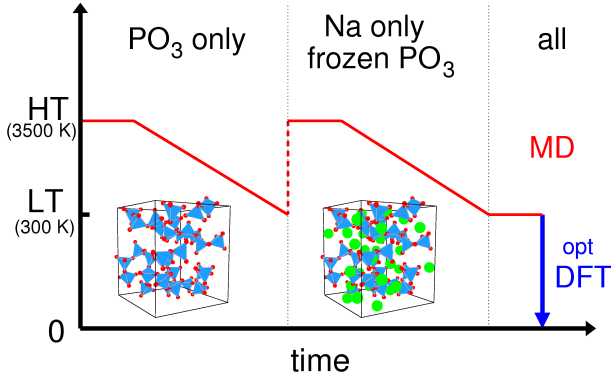


FIG. 3: (Color on-line) Schematic representation of the procedure used to obtain one configuration of sodium metaphosphate glass. From a well equilibrated trajectory at high temperature, the phosphate network is first quenched to a low temperature configuration. Then, the same quench rate is applied to the sodium atoms in the frozen phosphate “skeleton”. After a small equilibration trajectory at low temperature on all atoms, the DFT total energy of the configuration is minimised at 0 K. A total of 17 configurations were generated by this procedure.

approximated by:

$$|V_{zz}(0)| \propto \frac{\langle |V_{zz}| \rangle \sqrt{1 + \langle \eta_Q \rangle^2 / 3}}{\tau(\epsilon) \sqrt{1 + \eta_Q(0)^2 / 3}}$$

where $\tau(\epsilon)$ is a function given by Eq.15 of Ref. 35

The method described above involves only simple desk calculations. We notice that the deconvolution program of solid-state quadrupolar NMR spectra of Grimminck et al.⁴¹ uses a more precise method based on the bivariate distribution of the ECM expressed in the form of a triple integral.

III. THEORETICAL APPROACH

A. Sodium metaphosphate structural glass model

In the present work, we used a combination of classical molecular dynamics (MD) simulations and DFT calculations to generate a configuration manifold of the sodium metaphosphate glass system as schematized in Figure 3.

Basically, our approach is divided into two general steps: (i) the quench from a high-temperature configuration to a low temperature configuration using classical MD simulations and (ii) the energy minimisation of the final configuration within DFT (which can be seen as a quench to 0 K with infinite rate). In other words, the first step allows a quick sampling of different configuration space basins by fast classical MD. The second step allows to sample the “DFT local minima” of the potential energy landscape⁴². This latter step is essential to obtain accurate local geometries required to derive reliable NMR parameters¹³. However, as the size of the system is limited to about a hundred of atoms due to DFT-PAW/GIPAW calculation time, more than one glass configuration is required

to correctly sample the different NMR tensor distributions. Following the ergodic hypothesis, one can generate several configurations to accurately sample the configuration space to overcome this size limitation⁴³. Configurations extracted from low-temperature trajectories cannot be used in this aim as at low temperature, the structural reorganisations are too small and NMR parameters are limited to vibrational time averaging⁴⁴. Therefore, several quenches are needed.

As classical molecular dynamic simulations are based on empirical potentials, it is important to carefully check its ability to generate reliable structures before DFT optimisation. In case of oxide glasses, an important structural feature is the coordination of the different polyhedra commonly represented within the Q^n notation. For phosphates, n is the number of phosphate linked to a given phosphate group with $n \leq 4$. Thereafter, we call “secondary structure” this coordination structure property, opposed to “primary structure” (distances) which can be determined by radial distribution function analysis. This secondary structure is hardly modified at the *ab initio* step of our procedure, even if we consider an AIMD at low temperature⁴⁵. Indeed, the time scale currently available by AIMD is too short to induce such structural rearrangement. It is thus essential to correctly reproduce it at the classical MD level.

Experimentally it is known from ³¹P NMR that the binary sodium metaphosphate glass $((\text{Na}_2\text{O})_{1/2})(\text{P}_2\text{O}_5)_{1/2}$ is only composed by Q^2 (e.g. infinite phosphates chains)⁴⁶. It is also known that the Na_2O oxide play the role of network modifier. Indeed, an excess or a default of Na_2O oxide in sodium metaphosphate glasses arises to respectively an increase of Q^1 or Q^3 coordination⁴⁷.

In a preliminary study, we observed that the classical force-field chosen for this study (presented in next section) was unable to reproduce the experimental phosphate network of sodium metaphosphate, and this for any reachable order of magnitude of the quenching rate. This behaviour is largely dependent on the sodium charge involved in the long range electrostatic term. Indeed, we observed that decreasing the sodium charge leads to an increase of the Q^2 concentration. Surprisingly, the Q^2 concentration reaches the experimentally expected concentration when no sodium atoms were added at all. Consequently, we separated the classical molecular dynamics procedure into two steps, quenching first the phosphate network to obtain the correct Q^n concentration and then quenching the sodium cations in the fixed phosphate “skeleton”.

B. Force-Field and Thermal quenching procedure

Amorphous sodium metaphosphate configurations were generated using the effective force field proposed by van Beest, Kramer and van Santen (BKS)^{48,49}. This force-field, which is only based on two-body potential, is formalised by the following equation:

$$V_{\alpha\beta} = \frac{q_\alpha q_\beta}{r} + A_{\alpha\beta} \exp\left(-\frac{r}{\rho_{\alpha\beta}}\right) - \frac{C_{\alpha\beta}}{r^6} \quad (8)$$

Atomic pair	Force-Field parameters			
	$A_{\alpha\beta}$	$\rho_{\alpha\beta}$	$C_{\alpha\beta}$	q_{α} (charge)
Na–O	354.22072	0.24186	0.0	$q_{\text{Na}} (+1)$
P–O	903.4208	0.19264	1.98793	$q_{\text{P}} (+3.4)$
O–O	138.8773	0.36232	17.50	$q_{\text{O}} (-1.2)$

TABLE I: Force Field parameters used to generate MD trajectories in the classical step of the procedure. This force-field was proposed by van Beest, Kramer and van Santen (BKS)^{48,49} Units: energies are given in J/mol, distances in Å and charges in atomic units.

where the first term is the electrostatic interaction with partial charges q_{α} . The following two terms correspond to the Buckingham potential, which is composed by an exponential repulsive part and an r^{-6} attractive term. Table I summarizes the values of the set of parameters (q_{α} , $A_{\alpha\beta}$, $\rho_{\alpha\beta}$ and $C_{\alpha\beta}$) used in the classical step of our procedure for each α, β atomic pairs. The short-range part of the potential was truncated at 6.1 Å and Ewald sum method was used to deal with the long-range electrostatic forces. The form A of NaPO_3 crystalline compound⁵⁰ was chosen as an initial configuration for the MD simulation. We used a $2 \times 2 \times 1$ super-cell containing 160 atoms (32 ^{23}Na , 32 ^{31}P and 96 ^{17}O sites) with cell parameters set to $a = 12.20$ Å, $b = 12.48$ Å and $c = 14.07$ Å to match to the experimental density of the glass system with the same stoichiometry (2.53 g/ml).

The configurations are obtained by quenching different configurations extracted from a long well equilibrated high temperature trajectory (~ 1 ns at 3500K) to low temperature configurations (300K). The classical quench was obtained by 20 temperature steps in NVE ensemble (equilibrating for 2 ps at each step). The former quench procedure corresponds to a quenching rate of ~ 4 K/ps. The chosen quench rate is slow enough to reproduce final structures that provide NMR parameters in reasonable agreement with experiments and fast enough to be tractable in terms of computation time. Classical trajectories were obtained using the academic code DL_POLY⁵¹. Hundreds of configurations have been obtained by this procedure. Then, the atomic positions were optimised (e.g energy minimisation) with DFT calculations using the VASP code (Vienna Ab-initio Simulation Package)^{52–55}. These calculations were done at DFT-GGA (PW91)^{56–58} level of theory using standard PAW⁵⁹ to describe the electron-ion interactions. Plane-wave basis cut-off was set to ~ 44 Ry (600eV) and only the Γ -point was used in the Brillouin integration. The geometry was considered as converged when the forces acting on the atoms were below 0.01 eV/Å. This last step of the procedure being more time consuming, only a limited number of configurations could be generated. We finally generated 17 configurations of metaphosphate glass (NaPO_3) by this complete procedure giving us a statistical sampling of 544 sodium and phosphorus sites and 1632 oxygen sites.

	MD ^a	Neutron ^b	this study
Atomic pair	R (Å)	R (Å)	R (Å)
P–NBO	1.50	1.48	1.45
P–BO	1.59	1.61	1.65
P–P	3.18	2.93	2.95
O–O	2.51	2.52	2.55
Na–Na	3.10	3.07	3.35
Na–O	2.31	2.33	2.35
Coordination(%)			
Q ¹	25	-	4
Q ²	50	100 ^c	92
Q ³	25	-	4

^afrom Ref. 60

^bfrom Ref. 61

^cby definition of the metaphosphate structure

TABLE II: A comparison between some structural properties of our MD configurations and published data. (top) Position (R) of the first peak of the radial distribution function. (bottom) Phosphate coordination (Q^n) composition. Distances R are given with an uncertainty of ± 0.02 Å for the neutron study⁶¹ and of ± 0.025 for this work.

C. NMR tensor calculations

NMR tensor calculations were performed on the obtained configurations using the PARATEC code at DFT level of theory^{62,63}. We used the PBE⁶⁴ functional for the generalised gradient approximation (GGA) of the exchange-correlation functional. The potentials due to the ions are represented by norm-conserving Troullier-Martins pseudo-potentials⁶⁵. The electronic configuration involved in the construction of the pseudo-potentials for the different nuclei ^{23}Na , ^{31}P and ^{17}O are respectively $\{2p^2 2p^6 3d^0\}$, $\{3s^2 2p^{1.8} 3d^{0.2}\}$ and $\{2s^2 2p^3\}$ with respective core radii (in atomic unit) $\{1.8 1.49 1.8\}$, $\{2.0 2.0 2.0\}$ and $\{1.45 1.45\}$.

The electronic structure gives access to the EFG tensor through the reconstruction of the all-electron wavefunction that is obtained with the PAW approach.^{10,66} The non-diagonalised EFG tensor \mathbf{V} is used to calculate the five real components U_i (Eq. 2), whereas the principal components V_{xx} , V_{yy} and V_{zz} of the diagonal tensor are used to calculate the quadrupolar coupling constant C_Q and the asymmetry parameter η_Q (defined by relation 1). However, as mentioned above, V_{zz} will be used in the distribution analysis.

The calculation of the chemical shielding tensor was performed using the linear-response method⁶⁷ using the GIPAW reconstruction developed by Pickard and Mauri⁹. Experimental isotropic chemical shifts δ_{cs} and absolute isotropic chemical shielding σ are related through the definition of an isotropic reference shielding σ_{ref} defined by $\delta_{cs} = \sigma_{ref} - \sigma$. In the NMR community, it is commonly accepted to use a liquid as an external chemical shift reference. In the present work, we set the absolute chemical shift value to an unambiguous isolated resonance of a crystalline site studied previously³⁷.

For both EFG and CSA tensor calculations, we used an energy cutoff of 100 Ry, according to convergence tests previously performed on crystalline compounds^{37,68}. Owing to the

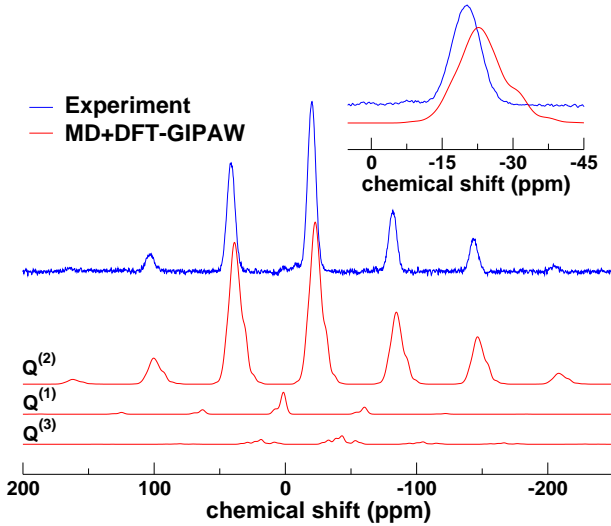


FIG. 4: (Color on-line) Experimental and simulated ^{31}P MAS spectrum of NaPO_3 at 18.8 T (MAS frequency is 20kHz). The simulated spectrum is obtained from DFT-GIPAW calculations on the MD configurations. The experimental spectrum shows small signals at 0 ppm assigned to Q^1 sites revealing an excess in Na_2O . (insert) Enlarged view of the isotropic region of the spectrum centered on the Q^2 region.

size of the unit cell, only one k-point was used for the integration of reciprocal space.

IV. RESULTS

A. Validation of the structural model

1. Local order and medium range order

Table II compares the short (i.e the position of the maximum of the first peak of the radial distribution function, R) and medium range order parameters (relative concentration of Q^n) of the NaPO_3 MD configurations obtained with the procedure described above. We also present a previous attempt by Speghini *et al.*⁶⁰ to reproduce sodium metaphosphate glass structure from classical molecular dynamics. Experimental neutron diffraction data from Pickup *et al.*⁶¹ are also included for comparison. First, our glass model is seen to reproduce accurately the local structure, as represented through simple local geometrical parameters such as R . Our structural parameters are in better agreement with the experimental ones than are those of Speghini *et al.* which were calculated only with a classical procedure. This is essentially due to the ab initio step in our calculation scheme. However, as discussed above, an accurate structural glass model for phosphorous compounds cannot be restricted to the sole aim of reproducing the local structure. It should also describe the medium range structure. Our procedure provides a way to keep the ratio of Q^1 and Q^3 at a low level to fit the experimental data, whereas for example, the relative concentration of Q^n , is not accurately

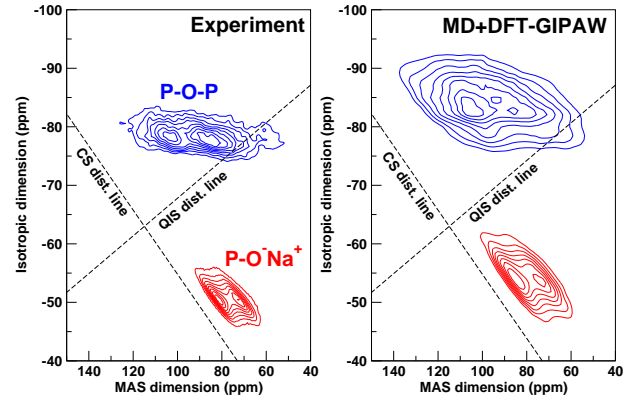


FIG. 5: (Color on-line) (left) Experimental and (right) theoretical ^{17}O MQMAS (calculated using MD configurations). BO and NBO oxygens are respectively represented in blue (top contour plots) and red (bottom contour plots). Chemical Shift (CS) and Quadrupolar Isotropic Shift (QIS) lines are represented by dashed lines.

reproduced in the work of Speghini *et al.* (see Table II).

2. Validation through ^{31}P and ^{17}O NMR

Figure 4 exhibits the experimental ^{31}P MAS NMR spectrum of NaPO_3 glass together with the one obtained from DFT-PAW/GIPAW calculation of NMR chemical shifts. The latter was obtained with 544 phosphorous sites. As expected, the main contribution occurs around -20 ppm, a chemical shift usually assigned to Q^2 groups. The experimental spectrum shows some very small resonances in the region of Q^1 phosphorous, revealing a small excess of sodium in the chemical composition as compared to the stoichiometric composition. On the simulated spectrum, the small resonances around 0 ppm and -40 ppm are due respectively to the Q^1 and Q^3 coordinations present in our statistical sampling. A close look at the simulated spectrum additionally reveals an overestimation of the ^{31}P Q^2 linewidth as well as a small shoulder around -30 ppm, revealing some limitations of our structural model.

Figure 5 compares experimental and simulated MQMAS spectra of NaPO_3 at 18.8T. It is important to recall that a MQMAS spectrum of an amorphous material gives the means to separate the chemical shift distribution from the distribution of quadrupolar parameters. Indeed, these distributions lead to a broadening of the two-dimensional site along two different axis, as evidenced in figure 5 (a). In the NBO region, we interpreted recently the broad distribution of chemical shift as a consequence of long-range disorder in contrast to the conservation of the local structure observed through the small spreading along the quadrupolar distribution axis.³⁷ The NBO and BO sites are experimentally clearly separated by their chemical shifts, quadrupolar coupling constants and to a lesser extend by their asymmetry parameters.

The NBO sites present a broad distribution in chemical shifts, which is well reproduced by the MD configurations that permit to reproduce the resonance asymmetry observed in the MAS dimension. On the other hand, for the BO, the

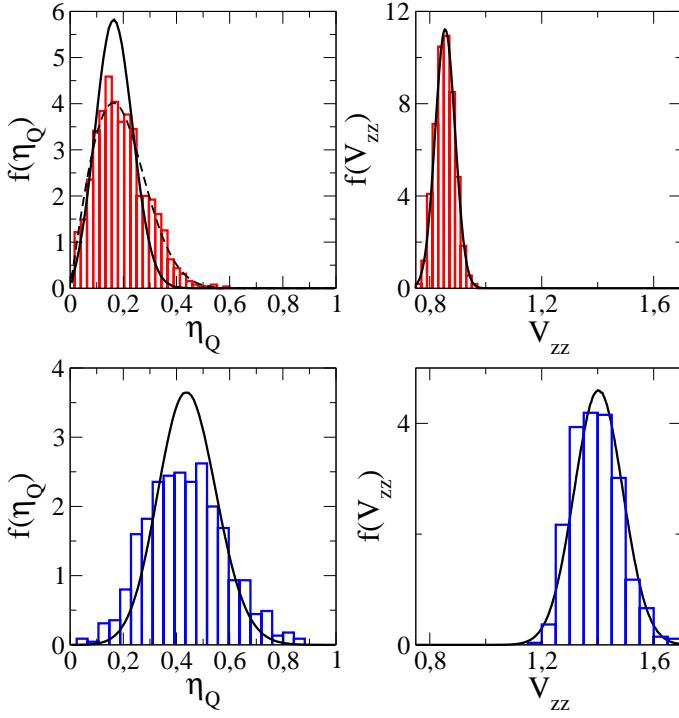


FIG. 6: (Color on-line) Distributions of η_Q and V_{zz} of ^{17}O NBO (top and red) and of ^{17}O BO (bottom and blue) for the MD configurations compared with the η_Q and V_{zz} distributions obtained from the ECM (black solid lines). The η_Q distribution obtained when distributing the ECM parameter $\eta_Q(0)$ according to a narrow Gaussian distribution ($\sigma^2 = 0.006$) is represented by the dashed line. The other ECM parameters are: ^{17}O NBO : $\eta_Q(0) = 0.15$, $V_{zz}(0) = 0.853$, $\epsilon = 0.093$. ^{17}O BO : $\eta_Q(0) = 0.43$, $V_{zz}(0) = 1.387$, $\epsilon = 0.135$.

line broadening in the MD spectrum reveals a broad distribution of chemical shift which seems to be overestimated with respect to the one observed experimentally. Overall, the main NMR parameters are well accounted for by the MD configurations for both BO and NBO sites.

B. ECM analysis of the EFG distribution

Table III gathers results obtained from the previous MD calculations and the ECM parameters deduced from the procedure described in section II C 2.

Sodium atoms in our MD configurations have $P(V_{zz} > 0) \approx P(V_{zz} < 0)$ as expected if the GIM holds. This suggests that the EFG distribution of these sites is a Czjzek distribution. However the ratio ρ_z (0.3487) is slightly larger than the Czjzek value of 0.32607. This difference is probably non-significant and related to the statistical fluctuations because of the low number of sites used to calculate it. In any case, the ECM analysis of sodium sites leads to the same parameters than those of the Czjzek model.

The calculated EFG tensors of the oxygen atoms show a clear difference between BO and NBO through the calculated ECM parameters, $V_{zz}(0)$ and $\eta_Q(0)$, as expected from the MD

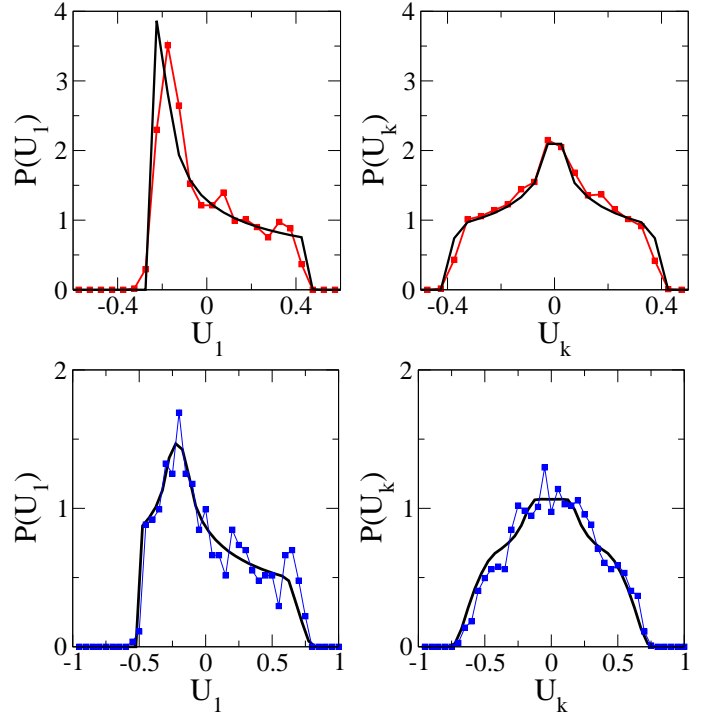


FIG. 7: (Color on-line) Distributions of U_1 and $U_{k,k>1}$ calculated for (top and red) ^{17}O NBO and (bottom and blue) ^{17}O BO from the MD configurations compared respectively to the "one point charge model" and to the "two point charge model" (black solid lines). The theoretical distributions are binned in the same way as the experimental ones. The parameters used to obtain the theoretical distributions (B 2 and B 1) of NBO and BO sites are respectively $\beta_0 = V_{zz}(0)/2 = 0.425$, 0.695 and $\eta_Q(0) = 0.15$, 0.43 .

structures. The important element here is that oxygen sites present only positive values of V_{zz} , differing strongly from the essentially equal weights of the positive and negative parts of the V_{zz} distribution which holds for the GIM. Furthermore, the ϵ values which are found to be small, being 0.09 and 0.13 for the NBO and BO, respectively, reflect a large local contribution in the ECM. Figure 6 presents the MD distributions of η_Q and V_{zz} parameters compared to the corresponding ECM distributions calculated with the parameters given in Table III. Small deviations between MD distributions and ECM analyses are observed for η_Q . This point will be addressed specifically in the next section. Finally, it is worth noting that such an overall agreement is obtained with a model based on three parameters only (i.e $V_{zz}(0)$, $\eta_Q(0)$ and ϵ).

V. STRUCTURAL INTERPRETATION OF THE DISTRIBUTIONS

The previous discussion concentrates on the distributions of the principal values of the EFG as calculated from our structural models. In this section, we focus on the distributions of the components of the EFG vector \mathbf{U} (Eq. 2). These distributions are characterized and compared with some simple model

	N sites	MD Statistics		ECM parameters		
		$P(V_{zz} > 0)$	ρ_z	ϵ	$V_{zz}(0)$	$\eta_Q(0)$
^{23}Na	544	$\sim 46\%$	0.349	-	0.148	-
^{17}O NBO	1088	100%	0.041	0.093	0.853	0.15
^{17}O BO	544	100%	0.061	0.135	1.387	0.43

TABLE III: Statistical properties of the MD configurations together with the ECM parameters obtained from the EFG distribution analysis. (atomic units for EFG)

predictions for the oxygen and sodium sites.

A. The case of oxygen (^{17}O)

The calculated EFG distribution can be explained in terms of the local structural features of BO and NBO sites. Indeed, the ECM analysis unveils the existence of a strong local contribution, consistent with the small coordination number of oxygen atoms. Intuitively, we understand that the electrostatic field felt locally by oxygen atoms is principally due to the variation of charge density induced by the chemical bonds shared with phosphorus. All other contributions can be considered as small perturbations to this “localised” anisotropy in the charge distribution. As a consequence, it makes sense to analyse the calculated ^{17}O EFG distribution with a simple model of effective point charges, as discussed for instance in Ref. 26. This model describes the probability distribution of the EFG created at the centre of a sphere by a random repartition of n point charges on its surface. For this purpose, we analyse the distribution of \mathbf{U} , the vector whose components are related to the elements of the EFG tensor through Eq. 2. In practice, the discrete charge model is equivalent to the calculation of the

five components of \mathbf{U} by the following classical relations:

$$\begin{aligned}
 U_1 &= \frac{1}{2} \sum_n (q_n/r_n^3) (3 \cos^2(\theta_n) - 1) \\
 U_2 &= \sqrt{3} \sum_n (q_n/r_n^3) \sin(\theta_n) \cos(\theta_n) \cos(\phi_n) \\
 U_3 &= \sqrt{3} \sum_n (q_n/r_n^3) \sin(\theta_n) \cos(\theta_n) \sin(\phi_n) \\
 U_4 &= \frac{\sqrt{3}}{2} \sum_n (q_n/r_n^3) \sin^2(\theta_n) \sin(2\phi_n) \\
 U_5 &= \frac{\sqrt{3}}{2} \sum_n (q_n/r_n^3) \sin^2(\theta_n) \cos(2\phi_n)
 \end{aligned} \tag{9}$$

where q_n and r_n, θ_n, ϕ_n are respectively the charge and the positions in spherical coordinates of the n th point charge.

Le Caër and Brand used this simple problem to exemplify the convergence of the distributions of the U_i 's ($i = 1, \dots, 5$) to the GIM distributions, that is to identical Gaussian distributions with variance σ^2 , when the number n of point charges increases. Numerical simulations were performed for $n = 2, 3, 4$ while the convergence to Gaussian distributions was proven when n goes to infinity. Actually, the five distributions converge rapidly to Gaussians which are excellent approximations for n larger than 4-5. The EFG distribution is then the one predicted by the Czjzek model. As required by the statistical invariance by rotation of the previous point charge problem (section II A and Ref. 26), the distribution of U_1 is found to be asymmetric while the distributions of the $U_{k,k>1}$ are identical and symmetric.

Figure 7 gives the distributions of the U_i components (U_1 and $U_{k,k>1}$) for the ^{17}O sites (BO and NBO) encountered in our NaPO_3 glass model. These distributions are compared to the discrete charge model described above. Using reduced units ($q_n = r_n = 1$), a unique scaling factor is needed to match the two distributions. The ^{17}O sites are analysed with one or two charges, in order to mimic either the single covalent bond of NBO or the two covalent bonds of BO.

The distribution obtained from a single charge accounts accurately for the distributions of the five U_i of NBO. A first conclusion is that these distributions are fully consistent with statistical isotropy of the EFG tensor as described in section II A. Second, these distributions are not very sensitive to a distribution of the scaling factor mentioned above. Indeed, Gaussian or uniform distributions of this factor do not change the central parts of the $P(U_k)$ distributions (figure 7 top, see further B 2 and figure 12). Further, $P(U_1)$ present a sharp

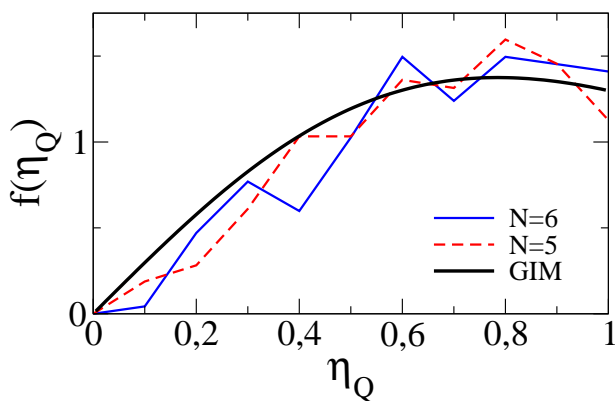


FIG. 8: (Color on-line) Distributions of η_Q of ^{23}Na in MD configurations for two different coordination numbers ($N = 5, 6$). These distributions are similar in shape to the Czjzek η_Q distribution (solid line). A similar trend is found for the other coordination numbers ($N = 4$ and 7) despite the limited number of atoms used to calculate them. (~ 50 sites).

peak on the left side as suggested by the distribution obtained from the MD-DFT calculations (figure 7). It is important to note that even if the marginal distributions $P(U_k)$ are correctly described by the previous model, the distribution of η_Q due to the effect of a single charge is a delta peak at $\eta_Q = 0$ in contradiction with the calculated one (figure 6). Indeed, the axial symmetry of the single point charge yields an asymmetry parameter equal to zero. Therefore, it is necessary to add a background to the EFG of this charge. Choosing a Czjzek EFG tensor to account for this background and expressing the total EFG tensor in the frame of reference of the EFG due to the single charge yields the ECM (Eq. 5). It is still an ECM in the presence of fluctuating scaling factors (see B). Moreover, the Czjzek background leaves essentially unchanged the U_i distributions. The latter have a rather limited discriminating power and are less suited than the distribution of η_Q to evidence fine effects. Slight changes of the EFG vector may have a weak incidence on the U distributions while they may produce significant changes of η_Q which is a ratio formed from them. This explains the higher sensitivity of the η_Q distribution. To summarize, the distributions of the U_1 and $U_{k,k>1}$ of the NBO are largely defined by local structural parameters (i.e., the number of covalent bonds shared with the phosphorus) whereas the distribution of the asymmetry parameter η_Q is influenced by second or more remote coordination spheres.

For BO sites, the distributions of the U_i 's can be reproduced by a two-charge model, where both charges mimic the anisotropy in the electronic structure produced by two covalent bonds. The resulting distributions are strongly dependent on the angle between the two charges and the centre of the sphere (i.e. angle POP). This strong dependence of the EFG distribution on the POP angle is consistent with a previous work of Clark *et al.*³⁸, revisited recently in a MD+DFT-GIPAW approach¹⁹, who established a correlation between the quadrupolar parameters and the Si—O—Si angle of ^{17}O BO, in silicate glasses. For the present two-charge model, only three parameters are needed to define the EFG tensor (five in the general case), correlating the principal components of the tensor (V_{zz} and η_Q). The observed EFG distributions can then be reduced to the distribution of two point charges with an effective angle. The distribution of the BO U_1 and $U_{k,k>1}$ are well accounted for by the EFG due to two charges with an angle deduced from the MD and DFT calculations. As above, the distributions $P(U_k)$ are fully consistent with the requirements of statistical isotropy (section II A). Distributions $P(U_{k,k>1})$ due to the effect of two charges making an angle 2θ differ just a little from those obtained from uniform distributions of the angle in domains $[2\theta_1, 2\theta_2]$ centered on 2θ with a width as large as 16° . These angle distributions leave essentially unchanged the distribution $P(U_1)$ (figure 7 bottom, see in addition B 1 and figure 11) except for the sharp peak which becomes rounded off. The ability of the $P(U_k)$ distributions to evidence fine effects is again less than it is for the η_Q distribution.

Finally, the analysis of the ECM distribution for the calculated ^{17}O EFG parameters shows some limitations to perfectly reproduce the η_Q distribution. This is partially due to the simplified way of modeling the local contribution to the full EFG

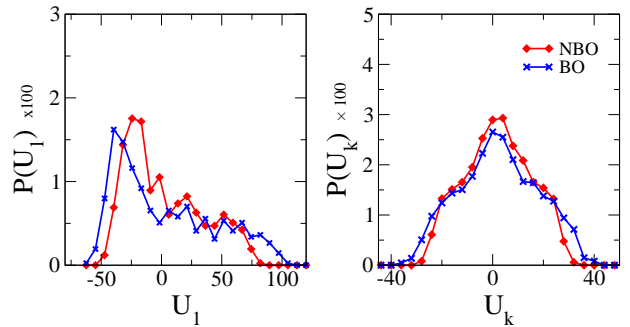


FIG. 9: (Color on-line) Distributions of U_1 and of $U_{k,k>1}$ for the CSA tensor calculated for ^{17}O NBO (red) and ^{17}O BO (blue) from the MD configurations.

tensor by a single fixed tensor (Eq. 5). Indeed, by simply considering a narrow gaussian distribution of $\eta_Q(0)$, it is possible to reproduce the observed η_Q distribution (left top dash-line Figure 6). This additional distribution of the anisotropic contribution could be interpreted as a small structural distribution of the local geometrical parameters (distances and angles).

In summary, the $P(U_k)$ are fully consistent with the statistical isotropy of the model glass. The modelling of the EFG tensors in terms of the contribution of one or of two charges with an additional Czjzek contribution from the background corresponds to the ECM (Eq. 5) provided that the local frame of reference is chosen to be the one associated with the single charge or the doublet of charges. However, the previous ECM distributions deduced from the MD+DFT calculated EFG parameters of ^{17}O atoms do not account perfectly for their η_Q distributions. This is partially due to a simplified modelling of the local contribution to the total ECM (section II C 1). As emphasized by Le Caër *et al.* in the conclusion of Ref. 35, a first step to make the ECM more realistic is to distribute the local contribution on a physical basis sound. Here, a narrow gaussian distribution of $\eta_Q(0)$ is indeed shown to suffice to account for fine details of the η_Q distribution calculated from the glass model as shown in figure 6 (dashed line, top left sub-figure).

B. The case of sodium (^{23}Na)

The ECM analysis of ^{23}Na sites reveals a trend of the EFG tensor of these nuclei to be distributed according to a Czjzek model. This observation was expected when considering the properties of a distributed point charge model as presented previously. Indeed, a structural analysis of the MD model reveals that sodium atoms have a distributed coordination number which ranges between 4 and 8, with more than 80% of them being 5- and 6-folded. For such coordinations, all the EFG components of the discrete charge model are normally distributed. Moreover, Figure 8 presents the distribution of η_Q for two sodium coordination numbers, $N = 5$ and 6, from our MD configurations. Both η_Q distributions show the general features of the GIM. Other coordination numbers ($N = 4$ and 7) also show the same trend despite the small sample size

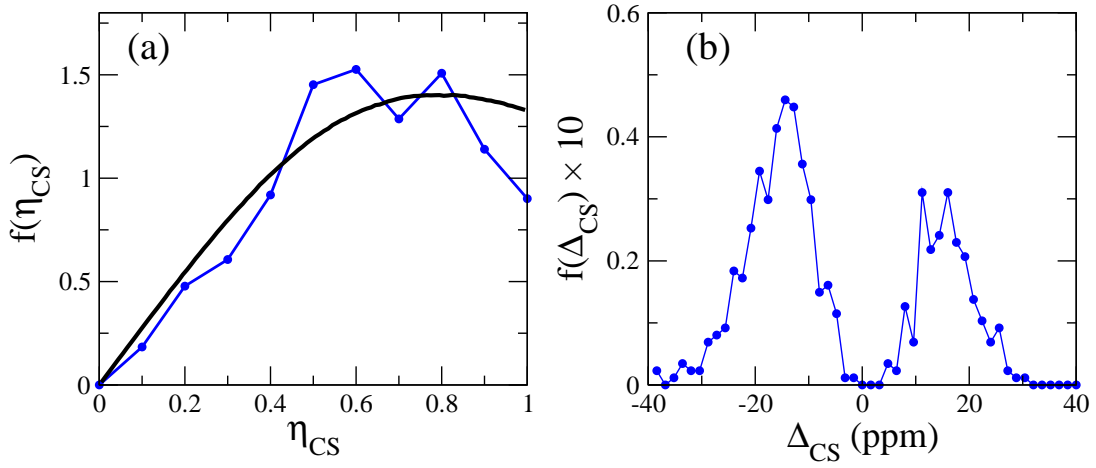


FIG. 10: Δ_{CS} and η_{CS} distributions of ^{23}Na of the MD configurations. These two distributions are similar in shape to those of the related Czjzek EFG distributions (see figure 1). The two parameters Δ_{CS} and η_{CS} play respectively the roles of V_{zz} et η_Q .

(*ca.* 50 sites for each coordination). More generally, these results confirm the statement that the GIM is valid when the coordination number is at least equal to 4.^{24,26}

VI. TOWARDS ECM ANALYSIS OF THE CSA TENSOR

Both the Czjzek model and the extended Czjzek model, which are based on quite general assumptions, are not restricted solely to the analysis of EFG tensors. Physical properties of statistically isotropic disordered solids which are represented in 3D space by symmetric second-rank tensors can be analysed in a way similar to the one performed in the present paper provided that the tensor elements are sums of various contributions to which the central limit theorem may apply. These physical properties may be measured or/and calculated from structural models. This is for instance the case of the deviatoric part of the atomic level stress tensor (ALS) in metallic glasses^{69,70} which was analyzed with a GIM in Ref. 71. The trace of the stress tensor is the local pressure whose distribution is approximately Gaussian⁶⁹. Similarly, the extended Czjzek model was applied to demagnetizing tensors to account for superparamagnetic resonance spectra of ferromagnetic particles in a diamagnetic matrix⁷².

The Chemical Shielding Anisotropy (CSA) tensor is worth being analyzed with the previous methods. In contrast to the EFG tensor, the CSA tensor has an isotropic part (non-zero trace) and is then completely determined by three parameters instead of two (V_{zz} and η_Q) for the EFG tensor. Within the Haeberlen convention,⁷³ we define the isotropic chemical shielding (σ_{iso}), the reduced anisotropy (Δ_{CS}) and the asymmetry parameter η_{CS} from the three principal components of

the CSA tensor (σ_{ii} , $i = 1, 2, 3$).

$$\sigma_{iso} = \frac{1}{3}(\sigma_{11} + \sigma_{22} + \sigma_{33}) \quad (10)$$

$$\Delta_{CS} = \sigma_{33} - \sigma_{iso} \quad (11)$$

$$\eta_{CS} = \frac{\sigma_{22} - \sigma_{11}}{\Delta_{CS}} \quad (12)$$

where the components σ_{ii} are sorted in the following way $|\sigma_{33} - \sigma_{iso}| \geq |\sigma_{11} - \sigma_{iso}| \geq |\sigma_{22} - \sigma_{iso}|$.

In the general case, the CSA tensor is completely characterized by six components. Five of them are defined by the five real U_i components given by Eq. 2, substituting $v_{\alpha\beta}$ by $\sigma_{\alpha\beta}$. The additional component, denoted as U_0 , corresponding to the isotropic parameter of the CSA interaction, is expressed by the following relation:

$$U_0 = -(1/\sqrt{3})(\sigma_{11} + \sigma_{22} + \sigma_{33}) \quad (13)$$

However, to preserve the conditions imposed by statistical isotropy, the U_1 component should be now defined by

$$U_1 = (1/2)(\sigma_{33} - \sigma_{iso}) \quad (14)$$

To illustrate the similarity between the CSA and EFG distributions, we analyzed the distribution of U_i for the CSA tensor of oxygen sites. The data were obtained from the DFT-GIPAW calculation of the NaPO_3 configurations generated by MD. First, as expected, the distribution of U_0 is well described by a gaussian, centered around the chemical shielding experimentally observed for both NBO and BO (not shown). Figure 9 shows the U_i distributions for the two oxygen environments, namely BO and NBO. The distributions of U_1 , for both oxygens, are asymmetric, as those observed for the EFG. The distributions of the remaining components have a symmetric shape which differs from a Gaussian. The distributions of figure 9 show clear similarities with those of figure 7. These results lead to the conclusion that the ^{17}O CSA distributions need more than the GIM to be described properly.

Therefore, the ECM analysis can be used to characterize the CSA distribution, revealing at the same time, the local structural information that is encoded into the anisotropic part of this interaction.

Figure 10 presents the distributions of η_{CS} and Δ_{CS} parameters for sodium nuclei in our MD structural model. A Czjzek-like feature is easily identified for the η_{CS} distribution, while the Δ_{CS} parameter presents an almost symmetrical distribution about zero, and is close to the shape of the V_{zz} distribution in the Czjzek model. Both results indicate clearly that the distribution of the CSA tensor obeys the two general assumptions which lead to the GIM.

VII. CONCLUSION

We applied a general multi-approach whose aim is to analyse and to model the NMR tensor distribution in disordered systems. This approach makes use of MD simulations and DFT calculations of NMR properties (i.e Electric Field Gradient (EFG) and Chemical Shift Anisotropy (CSA)) to provide both structural and NMR information. More important, this combined approach yields the full distributions of the considered tensors which cannot be measured experimentally in general. The distributions of the NMR interaction tensors are analysed through two different models: the Gaussian Isotropic Model (GIM) also known as the Czjzek model and an extension of it, the Extended Czjzek Model (ECM). We propose in particular a simple procedure to extract the main parameters of these models from a given tensor distribution.

We applied this procedure to a simple binary glass: the sodium metaphosphate (NaPO_3). Using the strong sensitivity of NMR to the structural atomic arrangement, we validated the structural models generated by MD comparing the theoretical NMR response to high-resolved Solid-State NMR experiments. The ECM was used to analyse the calculated distributions of the EFG of the two quadrupolar nuclei present in this system (i.e ^{23}Na and ^{17}O). The ECM analysis reveals the validity of the GIM in case of sodium, showing its broad applicability. As discussed in previous studies, the universal nature of such distributions (central limit theorem) makes the extraction of structural information very difficult. In case of oxygen, the tensor distributions are shown to be dominated by a large local contribution. A simple additional analysis based on discrete charge distributions showed indeed that simple structural information might be extracted from the distribution of the components U_i of the investigated tensors

Finally, from the simple observations made about the CSA tensor distributions of ^{17}O and ^{23}Na nuclei, it is clear that CSA and EFG tensors can be analysed with similar tools. In other words, both GIM and ECM analyses might be useful and relevant to discuss experimental and theoretical observations of CSA distributions.

Acknowledgments

Some of the numerical results presented in this paper were carried out using the regional computational cluster supported by Université Lille 1, CPER Nord-Pas-de-Calais/FEDER, France Grille and CNRS. We highly appreciate and thank the technical staff of the CRI-Lille 1 center for their strong and helpful support. IDRIS is also acknowledged for CPU allocation under project number x20080911849. FV was supported by the Ministère de l'Éducation Nationale de l'Enseignement Supérieure et de la Recherche. The FEDER, Région Nord Pas-de-Calais, Ministère de l'Éducation Nationale de l'Enseignement Supérieur et de la Recherche, CNRS, and USTL are acknowledged for financial support. FV would acknowledge previous support from the Stichting voor Fundamenteel Onderzoek der Materie (FOM).

Appendix A: Additional remarks on the ECM

All the ECM tensors $\mathbf{V}(\epsilon)$ are expressed in a local frame of reference which is chosen, without loss of generality, as the one in which \mathbf{V}_0 is diagonal and changes from atom to atom. By contrast, the distribution of the EFG tensor $\mathbf{V}'(\epsilon)$ (presented in B) of all “sites” belonging to the same family is calculated in a fixed global frame of reference identical for all atoms. It differs thus from the distribution of the tensor $\mathbf{V}(\epsilon)$ (Eq. 5). The spatial extent of a cluster around the considered atomic probe is expected to depend on the investigated solid and on the physical origins of the EFG (ex: close neighborhood for covalent glasses). The statistical isotropy of this family would mean that the previous clusters have an overall random orientation in the considered solid. This general property holds for any geometrical characteristics of these clusters. The only general a priori knowledge about the distribution of $\mathbf{V}'(\epsilon)$ at the cluster centers is that it depends on the invariants of the EFG tensor when statistical isotropy holds (see equations 7,8 and 10 of Ref. 25). In addition, the associated distributions $P(U'_k)$ fulfill the conditions described in section II A. To obtain the isotropic distribution of $\mathbf{V}'(\epsilon)$ from Eq. 5 , it would suffice to rotate the local frame of reference, defined from \mathbf{V}_0 , uniformly in all directions. The principal value distribution of $\mathbf{V}'(\epsilon)$ is identical with the principal value distribution of $\mathbf{V}(\epsilon)$ as further discussed in B. Eq. 5 suffices thus to derive the required information about the η_Q and V_{zz} distributions of the associated statistically isotropic EFG. A consequence of this choice is however that the distribution $P(\mathbf{U}')$, of $\mathbf{U}'(\epsilon)$ the vector associated with $\mathbf{V}'(\epsilon)$ (Eq. 2), cannot be derived directly from Eq. 5.

Appendix B: Rotation of the ECM tensor

Consider a particular tensor $\mathbf{V}(\epsilon)$ obtained by choosing at random some \mathbf{V}_{GIM} tensor in Eq. 5, $\mathbf{V}(\epsilon) = \mathbf{V}_0 + \rho(\epsilon)\mathbf{V}_{\text{GIM}}$, where \mathbf{V}_0 is diagonal. The considered symmetric second-rank tensor is transformed into a diagonal tensor $\mathbf{V}_D(\epsilon)$ by some

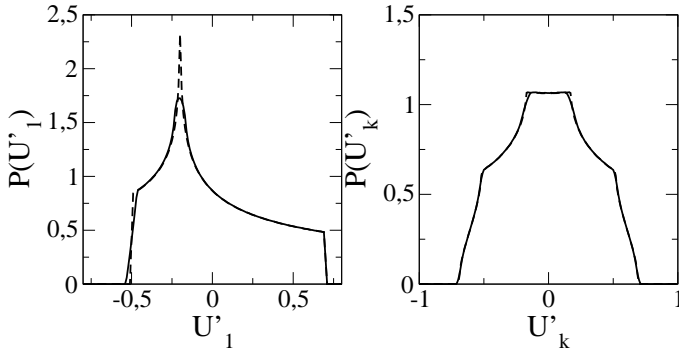


FIG. 11: Distribution of U'_1 and of $U'_{k,k>1}$ obtained with $\beta_0 = 0.7$ either with $\eta_Q(0) = 3/7$ (dotted lines) or with $\eta_Q(0)$ uniformly distributed between 0.33 and 0.53 (solid lines). The distribution of $P(U'_1)$ with a fixed $\eta_Q(0)$ is calculated from equations B6 and B7 while all the others distributions are calculated by Monte-Carlo simulations.

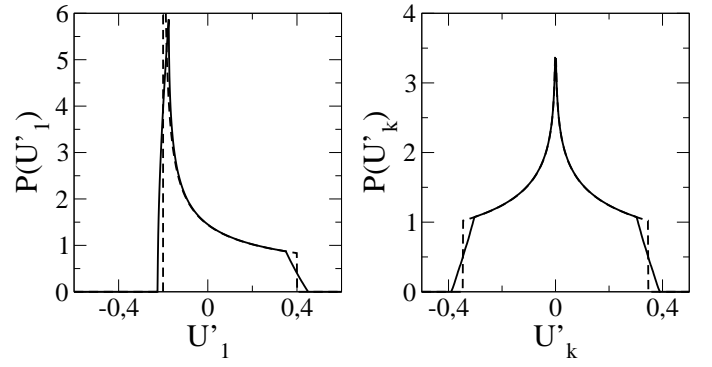


FIG. 12: Distributions of U'_1 and of $U'_{k,k>1}$ obtained from relations B12 and B13. The distributions are calculated for (dashed line) a fixed $\beta_0 = 0.4$ and (full line) a β_0 parameter uniformly distributed between 0.35 and 0.45.

rotation whose associated (3x3) matrix is H_0 , in matrix notation:

$$\mathbf{V}_D(\epsilon) = H_0 \mathbf{V}(\epsilon) H_0^T \quad (B1)$$

and thus, $\mathbf{V}_D(\epsilon) = H_0^T \mathbf{V}(\epsilon) H_0$, where H_0^T is the transpose of H_0 ($H_0 H_0^T = H_0^T H_0 = I$). The tensor $\mathbf{V}(\epsilon)$ is transformed by a rotation H_1 into a tensor $\mathbf{V}'(\epsilon)$:

$$\mathbf{V}'(\epsilon) = H_1 \mathbf{V}(\epsilon) H_1^T = H_1 H_0^T \mathbf{V}_D(\epsilon) H_0 H_1^T \quad (B2)$$

or equivalently:

$$\mathbf{V}'(\epsilon) = H_2 \mathbf{V}_D(\epsilon) H_2^T \quad (B3)$$

where $H_2 = H_1 H_0^T$ is a rotation matrix. The distribution of H_1 must be taken as uniform over the special orthogonal group $SO(3)$ to obtain a global statistical isotropy of the EFG tensor $\mathbf{V}'(\epsilon)$. The standard definition of uniformity requires the distribution of H_1 to remain unchanged when composed with any arbitrary rotation (Haar measure). Therefore, the distribution of H_2 is uniform too and the principal values of the tensors $\mathbf{V}'(\epsilon)$ and $\mathbf{V}(\epsilon)$ coincide with the diagonal elements of $\mathbf{V}_D(\epsilon)$. This line of reasoning can be applied to any tensor formed as above from Eq. 5. Thus, by construction, the global distribution of the EFG tensor $\mathbf{V}'(\epsilon)$ is statistically isotropic and its principal value distribution is identical with that of $\mathbf{V}(\epsilon)$. Therefore, the knowledge of the a priori complicated distribution of $\mathbf{V}'(\epsilon)$ is useless when only principal values matter. Equation 5 suffices to provide the required information about the η_Q and V_{zz} distributions of the associated statistically isotropic EFG tensor $\mathbf{V}'(\epsilon)$. However, by this choice, the distribution $P(\mathbf{U}'(\epsilon))$ cannot be derived without additional calculations based on Eq. B3. Simplified examples are given below to illustrate the need of more than a single family of sites to account for the EFG distribution of some disordered solids described by the ECM.

1. Uniform rotation

We consider the fixed diagonal part \mathbf{V}_0 of the ECM model (Eq. 5) which is expressed in its system of principal axes. The associated vector \mathbf{U}_0 has therefore only two non-zero components, namely $U_1(0) = V_{zz}(0)/2$ and $U_5(0) = \eta_Q(0)V_{zz}(0)/2\sqrt{3}$. When the principal axis system is rotated uniformly in all directions, the tensor \mathbf{V}_0 is transformed into a tensor \mathbf{V}'_0 whose elements are consequently distributed. By construction, the distribution of \mathbf{V}'_0 is then statistically isotropic and the components of the associated vector \mathbf{U}'_0 have marginal distributions which fulfill the conditions described in section II A. The distributions $P(U'_k(0))$ can be obtained either in closed form for $k = 1$ and for any k for $\eta_Q(0) = 0$ or by numerical simulations for any $k > 1$ as soon as $V_{zz}(0)$ and $\eta_Q(0)$ are known. These two parameters are obtained in the examples discussed below from simple physical models. This appendix aims to present the distribution of the first component $U'_1(0)$ of \mathbf{U}'_0 .

After a rotation of the previous frame of reference by the Euler angles α, β, γ , with $(0 \leq \alpha, \gamma < 2\pi, 0 \leq \beta < \pi)$, $U'_1(0)$ is directly calculated from the expressions given in B of Ref. 26 to be:

$$U'_1(0) = \frac{\beta_0}{2} (3 \cos^2(\beta) - 1 + \eta_Q(0) \sin^2(\beta) \cos(2\alpha)) \quad (B4)$$

with

$$-\rho_0 < U'_1(0) < \beta_0 \quad (B5)$$

where β_0 is some positive scale factor and $\rho_0 = \beta_0(1 + \eta_Q(0))/2$. To derive the sought-after distribution, it suffices therefore to consider a random rotation $(0 \leq \alpha < \pi/2, 0 \leq \beta < \pi/2)$ with a weight $(2/\pi) \sin \beta d\alpha d\beta$. Focusing on the angular part of Eq. B4 we obtain two integrals which depends on $\cos(2\alpha)$. The first integral is obtained when $U'_1(0) < \beta_0(\eta_Q(0) - 1)/2$ and the second when $U'_1(0) > \beta_0(\eta_Q(0) -$

1)/2. The final distribution reads ($z = U'_1(0)$)

$$\begin{cases} P(z) = {}_2F_1\left(\frac{1}{2}, \frac{1}{2}; 1; A\right) \left(4\beta_0\eta_Q(0)(\beta_0 - z)\right)^{-1/2} \\ -\rho_0 < z < \rho_0 - \beta_0 \end{cases} \quad (\text{B6})$$

$$\begin{cases} P(z) = {}_2F_1\left(\frac{1}{2}, \frac{1}{2}; 1; \frac{1}{A}\right) \left(2\beta_0(3 - \eta_Q(0))(\rho_0 + z)\right)^{-1/2} \\ \rho_0 - \beta_0 < z < \beta_0 \end{cases} \quad (\text{B7})$$

with

$$A = \left((3 - \eta_Q(0))(\rho_0 + z)\right) \left(2\eta_Q(0)(\beta_0 - z)\right)^{-1} \quad (\text{B8})$$

where ${}_2F_1(,;)$ is a hypergeometric function. The previous probability density function is discontinuous at $U'_1(0) = \rho_0 - \beta_0 = \beta_0(\eta_Q(0) - 1)/2$.

As a first example, we consider the case of two identical charges q_1 and q_2 are located at equal distances from an origin O at which the EFG is observed, with an angle $\widehat{q_1 O q_2} = 2\theta$. The asymmetry parameter is $\eta_Q(0) = 3\cos^2\theta/(2 - 3\cos^2\theta)$ when $\theta = \arccos(1/\sqrt{3}) < \theta < \pi/2$. If θ is taken equal to $\arccos(1/\sqrt{5}) \sim 63.4^\circ$, the angle between the two charges is then 126.8° and $\eta_Q(0) = 3/7 \sim 0.4286$. The distribution $P(U'_1(0))$, which is calculated in that way from Eqs. B6 and B7 for $\beta_0 = 0.70$ (Fig. 11), reproduces then the essential characteristics of the binned distribution $P(U'_1)$ shown in figure 7 for the case of two charges. As explained in section V A, contributions from fluctuations of \mathbf{V}_0 and from the Czjzek background must however be added to account for the details of $P(U'_1)$.

When $\eta_Q = 1$, the components U_1 and U_5 cannot be distinguished, except for a scale factor, because $V_{xx} = 0$ and $V_{yy} = -V_{zz}$. Therefore, the distribution $P(U'_1(0))$ must become symmetric as is $P(U'_5(0))$ when statistically isotropy holds. Indeed, $P(U'_1(0))$ reduces to

$$P(U'_1(0)) = \frac{{}_2F_1\left(\frac{1}{2}, \frac{1}{2}; 1; \frac{\beta_0 - |U'_1(0)|}{\beta_0 + |U'_1(0)|}\right)}{2\sqrt{\beta_0(\beta_0 + |U'_1(0)|)}} \quad (\text{B9})$$

for

$$-\beta_0 < U'_1(0) < \beta_0 \quad \text{as} \quad \rho_0 = \beta_0 \quad (\text{B10})$$

The latter distribution is similar to the distribution $P(U'_k)$ calculated for a single charge. Using the statistical invariance by rotation, the variance of $U'_1(0)$ is readily obtained to be :

$$\langle U'_1(0)^2 \rangle = \frac{\beta_0^2}{5} \left(1 + \frac{\eta_Q(0)^2}{3}\right) \quad (\text{B11})$$

2. The case of a single charge

As a second example, we consider the EFG at the nuclei of a given isotope which is determined by a single neighboring point charge and by more remote atomic shells whose total contribution is described by a Czjzek tensor. The \mathbf{V}_0 contribution to Eq. 5 is then due to this single charge. If the charge does not fluctuate in value and in distance from the considered atom, the total EFG is described by a single ECM (Eq. 5) with $\eta_Q(0) = 0$. If the charge fluctuates in value or/(and) in distance, then the EFG must be described by a distribution of ECM, all with $\eta_Q(0) = 0$. We focus below on the distribution of the sole local part. The effect of the addition of a small Czjzek noise is just a smoothing of the distributions shown in figure 12.

The marginal distributions of the components of $(U'_0 = (U'_1, \dots, U'_5))$, are obtained from Eq. 9 with $n = 1$ for a random distribution of θ and ϕ (with $P(\theta, \phi) = \frac{1}{4}\sin(\theta)d\theta d\phi$). The distribution of $P(U'_1)$ is asymmetrical as expected from the conditions given at the end of section II A and has a simple closed-form:

$$P(U'_1) = (3\beta_0^2 + 6\beta_0 U'_1)^{-1/2} \quad \left(-\frac{\beta_0}{2} < U'_1 < \beta_0\right) \quad (\text{B12})$$

where the proportionality constant β_0 is chosen here to be positive and is related to the characteristic parameters (i.e charge and distance) of the problem. By contrast, the distributions $P(U'_{k,k>1})$ are all identical and symmetric:

$$P(U'_k) = \frac{{}_2F_1\left(\frac{1}{2}, \frac{1}{2}; 1; \frac{\alpha - |U'_k|}{\alpha + |U'_k|}\right)}{2\sqrt{\alpha(\alpha + |U'_k|)}} \quad -\alpha < U'_k < \alpha \quad (\text{B13})$$

where $\alpha = \beta_0\sqrt{3}/2$ and ${}_2F_1(,;)$ is a hypergeometric function. In figure 12, we represent two examples of distributions obtained from Eqs. B12 and B13: with and without a uniform distribution of β_0 where β_0 is chosen to reproduce the characteristic distribution observed in our structural model (see the binned distribution, figure 7 top right, solid line).

3. A perturbed diamond lattice

A third example deals with a diamond lattice whose atomic positions are very slightly shifted with random displacements derived from an isotropic Gaussian distribution. For simplicity, we assume that the EFG is due to point charges located at the lattice sites. In addition, the EFG at any site of this perturbed diamond lattice is assumed to be essentially due to its four first neighbors while more remote shells contribute to a Czjzek background. We focus on the distribution of η_Q obtained from $\mathbf{V}(\epsilon)$ (Eq. 5). Indeed, although the principal values of $\mathbf{V}(\epsilon)$ have very small magnitudes, they suffice to change significantly η_Q as it is a ratio. An expansion of the EFG tensor in terms of the Gaussian atomic displacements gives a zero-order tensor \mathbf{V}_0 which comes from the tetrahe-

dral coordination of a site and a first-order EFG tensor whose elements are centered Gaussians. This expansion yields Eq. 5 as the first-order tensor is a Czjzek tensor by itself. When added to the background tensor, the sum is still a Czjzek tensor because the sum of two independent Czjzek tensors with parameters σ_1 and σ_2 is a Czjzek tensor whose parameter is $\sigma = \sqrt{\sigma_1^2 + \sigma_2^2}$. If all atoms are identical, $\mathbf{V}_0 = 0$ and the EFG distribution is then a Czjzek distribution. If two different atomic species A and B, with different charges q_A and q_B ($\Delta q = |q_A - q_B|$), are distributed at random on the lattice sites with a composition $A_x B_{1-x}$, without any change of the atomic positions, then the distribution of η_Q at the A nuclei is a mixture of three distributions:

- (i) a Czjzek distribution which comes from A atoms, denoted $A[A_4]$ and $A[B_4]$, which are surrounded respectively by 4A atoms and by 4B atoms, with a weight $(x^4 + (1-x)^4)$ ($V_{zz}(0) = 0$).
- (ii) an ECM distribution which originates from $A[A_3B]$ and $A[AB_3]$ atoms, with a weight $(4x^3(1-x) + 4x(1-x)^3)$ and $\eta_Q(0) = 0$ ($V_{zz}(0) \propto 2\Delta q$).
- (iii) an ECM distribution which arises from $A[A_2B_2]$ atoms,

with a weight $6x^2(1-x)^2$ and $\eta_Q(0) = 1$, ($V_{zz}(0) \propto \Delta q$).

In (ii) and (iii), the tensor \mathbf{V}_0 and the values of $\eta_Q(0)$ reflect the symmetries of the underlying tetrahedral shell. The previous example, although oversimplified, sketches however situations which are encountered in real semiconductors. Indeed, a recent ^{75}As and ^{69}Ga solid state NMR study of $\text{Al}_x\text{Ga}_{1-x}\text{As}$ thin films combines on the one hand experimental results and on the other structural modeling of disorder in the Ga and Al positions together with first-principles DFT calculations to obtain, among others, the EFG distributions at the tetrahedrally coordinated As sites (Ref. 32). Knijn *et al.* found that the EFG distributions at $\text{As}[\text{Al}_4]$, $\text{As}[\text{Ga}_4]$ sites are accurately described by the Czjzek distribution. In addition, they showed that the EFG distributions at the As sites $\text{As}[\text{Al}_1\text{Ga}_3]$, $\text{As}[\text{Al}_3\text{Ga}_1]$ and $\text{As}[\text{Al}_2\text{Ga}_2]$ are accurately described by extended Czjzek distributions whose $\eta_Q(0)$ are respectively 0, 0, 1 as above for symmetry reasons (Figure 13 of Ref. 32).

References

-
- * Current address: CEA, IRAMIS, SIS2M, CEA/CNRS UMR 3299 - Laboratoire de Structure et Dynamique par Résonance Magnétique F-91191 Gif-sur-Yvette cedex, France
 - ¹ W. H. Zachariasen, J. Am. Chem. Soc. **54**, 3841 (1932).
 - ² J. M. Gibson, Science **335**, 929 (2012).
 - ³ M. M. J. Treacy and K. B. Borisenko, Science **335**, 950 (2012).
 - ⁴ A. Samoson, E. Lippmaa, and A. Pines, Mol. Phys. **65**, 1013 (1988).
 - ⁵ A. Llor and J. Virlet, Chem. Phys. Lett. **152**, 248 (1988).
 - ⁶ L. Frydman and H. J. S., J. Am. Chem. Soc. **117**, 5367 (1995).
 - ⁷ A. Medek, J. S. Harwood, and L. Frydman, J. Am. Chem. Soc. **117**, 12779 (1995).
 - ⁸ G. Gan, J. Am. Chem. Soc. **122**, 3242 (2000).
 - ⁹ C. J. Pickard and F. Mauri, Phys. Rev. B **63**, 245101 (2001).
 - ¹⁰ M. Profeta, F. Mauri, and C. J. Pickard, J. Am. Chem. Soc. **125**, 541 (2003).
 - ¹¹ J. R. Yates, T. N. Pham, C. J. Pickard, F. Mauri, A. M. Amado, A. M. Gil, and S. P. Brown, J. Am. Chem. Soc. **127**, 10216 (2005).
 - ¹² C. J. Pickard, E. Salager, G. Pintacuda, B. Elena, and L. Emsley, J. Am. Chem. Soc. **129**, 8932 (2007).
 - ¹³ C. Gervais, M. Profeta, F. Babonneau, C. J. Pickard, and F. Mauri, J. Phys. Chem. B **108**, 13249 (2004).
 - ¹⁴ M. Profeta, M. Benoit, F. Mauri, and C. J. Pickard, J. Am. Chem. Soc. **126**, 12628 (2004).
 - ¹⁵ S. Rossano, F. Mauri, C. J. Pickard, and I. Farnan, J. Phys. Chem. B **109**, 7245 (2005).
 - ¹⁶ S. A. Ashbrook, A. J. Berry, D. J. Frost, A. Gregorovic, C. J. Pickard, J. E. Readman, and S. Wimperis, J. Am. Chem. Soc. **129**, 13213 (2007).
 - ¹⁷ T. Charpentier, S. Ispas, M. Profeta, F. Mauri, and C. J. Pickard, J. Phys. Chem. B **108**, 4147 (2004).
 - ¹⁸ M. Benoit, M. Profeta, F. Mauri, C. J. Pickard, and M. E. Tuckerman, J. Phys. Chem. B **109**, 6052 (2005).
 - ¹⁹ T. Charpentier, P. Kroll, and F. Mauri, J. Phys. Chem. C **113**, 7917 (2009).
 - ²⁰ G. Ferlat, T. Charpentier, A. P. Seitsonen, A. Takada, M. Lazzeri, L. Cormier, G. Calas, and F. Mauri, Phys. Rev. Lett. **101**, 065504 (2008).
 - ²¹ S. Ispas, T. Charpentier, F. Mauri, and D. R. Neuville, Solid State Sci. **12**, 183 (2010).
 - ²² M. Kibalchenko, J. R. Yates, and A. Pasquarello, J. Phys.: Condens. Matter **22**, 145501 (2010).
 - ²³ A. Pedone, T. Charpentier, and M. C. Menziani, Phys. Chem. Chem. Phys. **12**, 6054 (2010).
 - ²⁴ J. B. d'Espinose de Lacaillerie, C. Fretigny, and D. Massiot, J. Magn. Reson. **192**, 244 (2008).
 - ²⁵ G. Czjzek, J. Fink, F. Götz, H. Schmidt, J. M. D. Coey, J.-P. Rebouillat, and A. Liénard, Phys. Rev. B **23**, 2513 (1981).
 - ²⁶ G. Le Caër and R. A. Brand, J. Phys.: Condens. Matter **10**, 10715 (1998).
 - ²⁷ M. E. Lopez-Herrera, J. M. Greneche, and F. Varret, Phys. Rev. B **28**, 4944 (1983).
 - ²⁸ D. R. Neuville, L. Cormier, and D. Massiot, Geochim. Cosmochim. Acta **68**, 5071 (2004).
 - ²⁹ V. Sabarinathan, S. Ramasamy, and S. Ganapathy, J. Phys. Chem. B **114**, 1775 (2010), pMID: 20073527.
 - ³⁰ B. Bureau, G. Silly, J. Y. Buzaré, C. Legein, and D. Massiot, Solid State Nucl. Magn. Reson. **14**, 181 (1999).
 - ³¹ B. Bureau, G. Silly, J. Y. Buzaré, B. Boulard, and C. Legein, J. Phys.: Condens. Matter **12**, 5775 (2000).
 - ³² P. J. Knijn, P. J. M. van Bentum, E. R. H. van Eck, C. Fang, D. L. A. G. Grimminck, R. A. de Groot, R. W. A. Havenith, M. Marsman, W. L. Meerts, G. A. de Wijs, et al., Phys. Chem. Chem. Phys. **12**, 11517 (2010).
 - ³³ C. Mellier, F. Fayon, V. Schnitzler, P. Deniard, M. Allix, S. Quillard, D. Massiot, J.-M. Boulard, B. Bujoli, and P. Janvier, Inorg.

- Chem. **50**, 8252 (2011).
- ³⁴ J. D. Epping, W. Strojek, and H. Eckert, *Phys. Chem. Chem. Phys.* **7**, 2384 (2005).
 - ³⁵ G. Le Caër, B. Bureau, and D. Massiot, *J. Phys.: Condens. Matter* **22**, 065402 (2010).
 - ³⁶ G. Le Caër, R. A. Brand, and K. Dehghan, *J. Physique Coll.* **46**, C8 (1985).
 - ³⁷ F. Vasconcelos, S. Cristol, J.-F. Paul, G. Tricot, J.-P. Amoureux, L. Montagne, F. Mauri, and L. Delevoye, *Inorg. Chem.* **47**, 7327 (2008).
 - ³⁸ T. M. Clark, P. J. Grandinetti, P. Florian, and J. F. Stebbins, *Phys. Rev. B* **70**, 064202 (2004).
 - ³⁹ P. Pykkö, *Mol. Phys.* **99**, 1617 (2001).
 - ⁴⁰ A. Abragam, *Les principes du magnétisme nucléaire* (Bibliothèque des sciences et techniques nucléaires, Saclay, 1961).
 - ⁴¹ D. A. G. Grimminck, B. J. W. Polman, A. P. M. Kentgens, and W. L. Meerts, *J. Magn. Reson.* **211**, 114 (2011), ISSN 1090-7807.
 - ⁴² P. G. Debenedetti and F. H. Stillinger, *Nature* **410**, 259 (2001).
 - ⁴³ R. M. Van Ginhoven, H. Jónsson, and L. R. Corrales, *Phys. Rev. B* **71**, 024208 (2005).
 - ⁴⁴ I. De Gortari, G. Portella, X. Salvatella, V. Bajaj, P. van der Wel, J. Yates, M. Segall, C. Pickard, M. Payne, and M. Vendruscolo, *J. Am. Chem. Soc.* **132**, 5993 (2010).
 - ⁴⁵ A. Tilocca and N. H. de Leeuw, *J. Phys. Chem. B* **110**, 25810 (2006), pMID: 17181225.
 - ⁴⁶ R. K. Brow, *J. Non-Cryst. Solids* **263**, 1 (2000).
 - ⁴⁷ M. Zeyer, L. Montagne, V. Kostoj, G. Palavit, D. Prochnow, and C. Jaeger, *J. Non-Cryst. Solids* **311**, 223 (2002).
 - ⁴⁸ B. W. H. van Beest, G. J. Kramer, and R. A. van Santen, *Phys. Rev. Lett.* **64**, 1955 (1990).
 - ⁴⁹ G. J. Kramer, N. P. Farragher, B. W. H. van Beest, and R. A. van Santen, *Phys. Rev. B* **43**, 5068 (1991).
 - ⁵⁰ A. McAdam, H. Jost, and B. Beagley, *Acta Crystallogr. B* **24**, 1621 (2007).
 - ⁵¹ [http : //www.ccp5.ac.uk/DL_POLY](http://www.ccp5.ac.uk/DL_POLY).
 - ⁵² G. Kresse and J. Furthmüller, *Comput. Mat. Sci.* **6**, 15 (1996).
 - ⁵³ G. Kresse and J. Furthmüller, *Phys. Rev. B* **54**, 11169 (1996).
 - ⁵⁴ G. Kresse and J. Hafner, *Phys. Rev. B* **49**, 14251 (1994).
 - ⁵⁵ G. Kresse and J. Hafner, *Phys. Rev. B* **48**, 13115 (1993).
 - ⁵⁶ J. P. Perdew, K. Burke, and Y. Wang, *Phys. Rev. B* **54**, 16533 (1996).
 - ⁵⁷ J. P. Perdew, J. A. Chevary, S. H. Vosko, K. A. Jackson, M. R. Pederson, D. J. Singh, and C. Fiolhais, *Phys. Rev. B* **46**, 6671 (1992).
 - ⁵⁸ J. P. Perdew, J. A. Chevary, S. H. Vosko, K. A. Jackson, M. R. Pederson, D. J. Singh, and C. Fiolhais, *Phys. Rev. B* **48**, 4978 (1993).
 - ⁵⁹ G. Kresse and D. Joubert, *Phys. Rev. B* **59**, 1758 (1999).
 - ⁶⁰ A. Speghini, E. Sourial, T. Peres, G. Pinna, M. Bettinelli, and J. A. Capobianco, *Phys. Chem. Chem. Phys.* **1**, 173 (1999).
 - ⁶¹ D. M. Pickup, I. Ahmed, P. Guerry, J. C. Knowles, M. E. Smith, and R. J. Newport, *J. Phys.: Condens. Matter* **19**, 415116 (2007).
 - ⁶² B. Pfrommer, D. Raczowski, A. Canning, S. G. Louie, F. Mauri, M. Cote, Y. Yoon, C. J. Pickard, and P. Heynes, PARATEC (PAR-Allen Total Energy Code).
 - ⁶³ W. Kohn and L. J. Sham, *Phys. Rev.* **140**, 1133 (1965).
 - ⁶⁴ J. P. Perdew, K. Burke, and M. Ernzerhof, *Phys. Rev. Lett.* **77**, 3865 (1996).
 - ⁶⁵ N. Trouillier and J. L. Martins, *Phys. Rev. B* **43**, 1993 (1991).
 - ⁶⁶ P. E. Blöchl, *Phys. Rev. B* **50**, 17953 (1994).
 - ⁶⁷ F. Mauri, B. G. Pfrommer, and S. G. Louie, *Phys. Rev. Lett.* **77**, 5300 (1996).
 - ⁶⁸ F. Vasconcelos, S. Cristol, J.-F. Paul, L. Montagne, F. Mauri, and L. Delevoye, *Magn. Res. Chem.* **48**, S142 (2010).
 - ⁶⁹ D. Srolovitz, K. Maeda, S. Takeuchi, T. Egami, and V. Vitek, *J. of Phys. F: Met. Phys.* **11**, 2209 (1981).
 - ⁷⁰ T. Egami, *Intermetallics* **14**, 882 (2006).
 - ⁷¹ G. Le Caër, J. M. Dubois, and R. A. Brand, *Amorphous Metals and Non Equilibrium Processes* (M. von Allmen, Les Ulis: Editions de Physique, Paris, 1984).
 - ⁷² J. Kliava and R. Berger, *J. Magn. Magn. Mater* **205**, 328 (1999).
 - ⁷³ U. Haeblerlen, *High Resolution NMR in Solids: Selective Averaging* (Academic press, USA, 1976).